Selective Nucleation and Discovery of Organic Polymorphs through Epitaxy with Single Crystal Substrates

Christine A. Mitchell,[†,‡] Lian Yu,*[,†] and Michael D. Ward*[,‡]

Contribution from the Lilly Research Laboratories, Eli Lilly and Company, Lilly Corporate Center, Indianapolis, Indiana 46285, and the Department of Chemical Engineering and Materials Science, University of Minnesota, Amundson Hall, 421 Washington Avenue SE, Minneapolis, Minnesota 55455

Received November 27, 2000. Revised Manuscript Received May 1, 2001

Abstract: Crystallization of 5-methyl-2-[(2-nitrophenyl)amino]-3-thiophenecarbonitrile (**1**), previously found to produce six conformational polymorphs from solution, on single-crystal pimelic acid (PA) substrates results in selective and oriented growth of the metastable "YN" (yellow needle) polymorph on the $(101)_{PA}$ faces of the substrate. Though the freshly cleaved substrate crystals expose $(101)_{PA}$ and $(111)_{PA}$ faces, which are both decorated with $[10\bar{1}]_{PA}$ ledges that could serve as nucleation sites, crystal growth of YN occurs on only $(101)_{PA}$. Goniometry measurements performed with an atomic force microscope reveal that the $(001)_{YN}$ plane contacts $(101)_{PA}$ with a crystal orientation $[100]_{YN}||[010]_{PA}$ and $[010]_{YN}||[10\bar{1}]_{PA}$. A geometric lattice analysis using a newly developed program dubbed GRACE (geometric real-space analysis of crystal epitaxy) indicates that this interfacial configuration arises from optimal two-dimensional epitaxy and that among the six polymorphs of **1**, only the YN polymorph, in the observed orientation, achieves reasonable epitaxial match to $(101)_{PA}$. The geometric analysis also reveals that none of the polymorphs, including YN, can achieve comparable epitaxial match with $(111)_{PA}$, consistent with the absence of nucleation on this crystal face. In contrast, sublimation of **1** on cleaved succinic acid (SA) substrates, which expose large $(010)_{SA}$ faces decorated with steps along $[10\bar{1}]_{SA}$, affords growth of several polymorphs, each with multiple orientations, as well as oriented crystals of a new metastable polymorph on the $(010)_{SA}$ surfaces. The lack of polymorphic selectivity on $(010)_{SA}$ can be explained by the geometric lattice analysis, which reveals low-grade epitaxial matches between $(010)_{SA}$ and several polymorphs of **1** but no inherent selectivity toward a single polymorph. These observations demonstrate the sensitivity of crystal nucleation to substrate surface structure, the potential of crystalline substrates for selective nucleation and discovery of polymorphs, and the utility of geometric lattice modeling for screening of substrate libraries for controlling polymorphism.

Introduction

Polymorphism, the ability of a molecule to adopt different crystal forms, reflects the delicate balance of forces responsible for guiding molecular organization in the solid state. Though often viewed as an annoyance, this phenomenon represents an opportunity to examine subtle structure−property relationships and the relationship between molecular conformation and crystal packing. Its elucidation promises molecular-level control of crystallization and improvement in crystal structure design and prediction. Polymorphism also has considerable technological significance owing to the dependence of crystal properties on solid-state structure. For example, the discovery and characterization of the polymorphs of a drug are important for evaluation of shelf stability (against transformations to other polymorphs) and bioavailability of the final pharmaceutical product.[1−4] Polymorph screening is a particularly important component of drug development processes because of patent protection of new crystal forms, regulations that require polymorph identification and characterization,[5] and the need for strict monitoring and recording of process conditions to achieve controlled and reproducible crystallization outcomes.[6] Despite decades of polymorphism studies,[2,3,7,8] prediction of all possible polymorphs of a given substance remains difficult. Furthermore, it is impossible to guarantee that all experimental parameters that could lead to the discovery of unknown forms have been exhausted,[9] or that polymorphs produced through an ostensibly reliable process will not disappear at a later time.[10]

Polymorph searching is typically achieved through a screening process in which a compound is crystallized in various solvents or combinations of solvents under various process conditions (e.g., rate of cooling of saturated solutions, evaporation of solvent, controlled addition of cosolvents). The small free energy differences between polymorphs (∼1 kcal/mol),[11] however,

* To whom correspondence should be addressed.
† Lilly Research Research Laboratories.
‡ University of Minnesota.

(1) Yu, L.; Reutzel, S. M.; Stephenson, G. A. *Pharm. Sci. Technol. Today* **1998**, *1*, 118−127.
(2) Habelian, J.; McCrone, W. *J. Pharm. Sci.* **1969**, *58*, 911−929.
(3) McCrone, W. Polymorphism. In *Physics and Chemistry of the Solid State*; Fox, D., Labes, M. M., Weissburger, A., Eds.; Interscience: New York, 1965; Vol. II, Chapter 8.
(4) *Polymorphism in Pharmaceutical Solids*; Brittain, H. G., Ed.; Marcel Dekker Inc.: New York,1999.
(5) Byrn, S. R.; Pfeiffer, R.; Ganey, M.; Hoiberg, C.; Poochikian, G. *Pharm. Res.* **1995**, *12*, 945−954.
(6) Rodríguez-Hornedo, N.; Murphy, D. *J. Pharm. Sci.* **1999**, *88*, 651−660.
(7) Threfall, T. L. *Analyst* **1995**, *120*, 2435−2460.
(8) Brittain, H. G. *J. Pharm. Sci.* **1997**, *86*, 405−412.
(9) Bernstein, J. *J. Phys. D: Appl. Phys.* **1993**, *26*, B66−B76.
(10) Dunitz, J. D.; Bernstein, J. *Acc. Chem. Res.* **1995**, *28*, 193−200.
(11) (a) Kitaigorodsky, A. I. *Molecular Crystals and Molecules*; Academic Press: New York, 1973. (b) Yu, L. *J. Pharm. Sci.* **1995**, *84*, 966−974.

10.1021/ja004085f CCC: $20.00
Published on Web 10/12/2001

commonly frustrate the achievement of good selectivity toward a desired form. Given that only one polymorph corresponds to the global thermodynamic minimum at one temperature, strategies for controlling polymorphism must rely on the manipulation of nucleation and crystal growth kinetics.

Several approaches for controlling nucleation and growth of organic crystals based on carefully designed growth interfaces have been reported recently, with these techniques relying on specific or epitaxial interactions between a nucleation-promoting surface and prenucleation aggregates of the crystallizing material, wherein the molecular organization in the prenucleation aggregate is presumed to be identical to that of the target crystal. Nucleation-promoting surfaces have included polymers,[12] Langmuir monolayers,[13] organic salt crystals,[14] graphite,[15] organic single crystals,[16] and surfaces of metastable crystal phases.[17] These approaches usually hinge on two-dimensional epitaxy, in which the nucleation interface contains a pair of low index lattice vectors of the nucleant that coincide with a pair of low index directions on the promoting substrate. The existence of an epitaxial condition generally is surmised from the orientation of the mature crystal on the substrate.

Related molecular level strategies for controlling polymorphism have been reported recently. "Designer" additives that interact with prenucleation aggregates of one polymorph can inhibit their growth so that the production of others is promoted.[18] Organosilane monolayers on glass surfaces can be used to manipulate polymorph selectivity.[19] One of our laboratories demonstrated that specific crystal faces of organic single crystals can be used as substrates to control polymorph selectivity through "ledge-directed epitaxy" (LDE),[20] wherein the free energy of a prenucleation aggregate, corresponding to a particular polymorphic form, is reduced by a shape-fitting contact with two planes of a crystallographically well-defined ledge site. This demonstrated the utility of organic crystals as substrates for controlling nucleation of crystalline materials. In principle, combinatorial-like searches for new polymorphs can be performed using libraries of organic crystal substrate seeds,[21] assembled from the substantial number of crystallographically characterized molecular crystals (>160 000 structures reported in the Cambridge Structural Database as of July 1, 2000). Related libraries could be built from inorganic materials, particularly those that naturally adopt layered structures. Such libraries can be devised more intelligently, and searches can be more efficient, if initial screens are based on geometric modeling of epitaxy, based on either LDE or two-dimensional (2-D) lattice matching, between contacting planes of the substrate and nucleant. The development of this strategy, however, first requires proof-of-principle based on a selected set of substrates and nucleants.

Herein, we describe the crystallization of 5-methyl-2-[(2-nitrophenyl)amino]-3-thiophenecarbonitrile (**1**) on organic crystal substrates. This compound, a precursor to the antipsychotic agent olanzapine,[22] forms six conformational polymorphs that, in addition to X-ray diffraction, are distinguishable by color, vibrational spectroscopy, and morphology.[23] The different colors of these polymorphs stem from the conformational isomerism of **1**, which produces varying degrees of conjugation between the phenyl and thiophene rings. Control of polymorphism for **1**

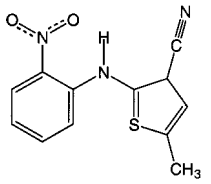

1

proved to be challenging; for example, several polymorphs crystallize concomitantly from methanol, and the desired polymorph can only be obtained after numerous trials and through careful introduction of seeds. The existence of numerous, well-characterized polymorphs and the sensitivity of polymorph selectivity to crystallization conditions make this system ideally suited for studying the effect of epitaxy, using foreign substrates, on polymorphic selectivity. Substrates capable of directing nucleation toward a specific polymorph can be valuable if seeds of that polymorph are not readily available. Furthermore, substrate libraries may lead to the discovery of new polymorphs that may not be produced using more conventional crystallization protocols.

We demonstrate here that crystallization of **1** on freshly cleaved single-crystal pimelic acid (PA) substrates, achieved here by sublimation methods, produces only the metastable "YN" (yellow needle) form as oriented needles on the $(101)_{PA}$ faces of the substrate. Though the PA substrates expose both $(101)_{PA}$ and $(111)_{PA}$ faces, crystal growth of YN occurs selectively on $(10\bar{1})_{PA}$, even though both faces contain ledges oriented along $[10\bar{1}]_{PA}$ that could serve as nucleation sites. This argues that the oriented growth and selectivity for YN on $(101)_{PA}$ surfaces stem from two-dimensional epitaxy, rather than LDE or nonspecific wetting of the step sites. In contrast, $(010)_{SA}$ faces of succinic acid (SA) substrates promote the simultaneous growth of several polymorphs of **1**, including oriented crystals of a previously unknown unstable polymorph. Geometric analyses of the numerous possible nucleation interfaces, comprising these selected substrates and a range of *hkl* planes of the known polymorphs, with a newly devised program dubbed GRACE (geometric real-space analysis of crystal epitaxy), confirm the existence of the two-dimensional epitaxy responsible for the selective nucleation of YN on $(101)_{PA}$ and, conversely, the absence of comparable lattice matches on the dormant substrate surfaces. Though crystal nucleation can be influenced by other factors (different inherent nucleation rates of polymorphs, relative growth rates of different crystal planes, Ostwald's rule of stages for polymorph nucleation, and solvent effects), this study demonstrates that epitaxy, which can be reliably predicted with geometric lattice modeling routines such as GRACE, can be a controlling influence on the selective nucleation of polymorphs. These observations further demon-

(12) Damman, P.; Dosière, M.; Smith, P.; Wittmann, J. C. *J. Am. Chem. Soc*. **1994**, *117*, 1117−1120.
(13) Frostman, L. M.; Ward, M. D. *Langmuir* **1997**, *13*, 330−337.
(14) DaCosta, V.; Le Moigne, J.; Oswald, L.; Pham, T. A.; Thierry, A. *Macromolecules* **1998**, *31*, 1635−1643.
(15) Last, J. A.; Hillier, A. C.; Hooks, D. E.; Maxson, J. B.; Ward, M. D. *Chem. Mater*. **1998**, *10*, 422−437.
(16) Carter, P. W.; Ward, M. D. *J. Am. Chem. Soc*. **1993**, *115*, 11521−11535.
(17) Rodríguez-Hornedo, N.; Lechuga-Ballesteros, D.; Wu, H.-J. *Int. J. Pharm*. **1992**, *85*, 149−162.
(18) (a) Staab, E.; Addadi, L.; Leiserowitz, L.; Lahav, M. *Adv. Mater*. **1990**, *2*, 40−43. (b) Weissbuch, I.; Lahav, M.; Leiserowitz, L. *Adv. Mater*. **1994**, *6*, 952−956. (c) Davey, R. J.; Blagden, N.; Potts, G. D.; Docherty, R. *J. Am. Chem. Soc*. **1997**, *119*, 1767−1772.
(19) Carter, P. W.; Ward, M. D. *J. Am. Chem. Soc*. **1994**, *116*, 769−770.
(20) Bonafede, S. J.; Ward, M. D. *J. Am. Chem. Soc*. **1995**, *117*, 7853−7861.
(21) Ward, M. D. *Curr. Op. Colloid Interface Sci*. **1997**, *2*, 51−64.
(22) Lilly Industries Limited, Kingsclere Road, Basingstoke Hants RG21 2XA, U.K. Eur. Pat. 0 454 436 A1, Bulletin 91/44, Oct 30, 1991.
(23) Yu, L.; Stephenson, G. A., Mitchell, C. A.; Bunnell, C. A.; Snorek, S. V.; Bowyer, J.; Borchardt, T. B.; Stowell, J. G.; Byrn, S. R. *J. Am. Chem. Soc*. **2000**, *122*, 585−591.

strate the sensitivity of crystal nucleation to substrate surface structure, the potential of crystalline substrates for controlling polymorphism and discovering new polymorphs, and the utility of geometric lattice modeling for screening of substrate libraries for polymorph control.

Experimental Section

Materials. Pimelic acid (PA) and succinic acid (SA) were obtained from the Aldrich Chemical Co. and used without further purification. The compound 5-methyl-2-[(2-nitrophenyl)amino]-3-thiophenecarbonitrile (**1**) was available from Eli Lilly and Company.[24] Slow evaporation of aqueous solutions of PA (1 g PA/25 mL H_2O) and SA (9 g SA/130 mL H_2O) at room temperature afforded crystals that could be cleaved to expose fresh growth surfaces. The PA crystals were plates 3−5 mm wide and 0.5−1.0 mm thick with large $\{100\}_{PA}$ faces and smaller $\{101\}_{PA}$, $\{001\}_{PA}$, $\{10\bar{1}\}_{PA}$, and $\{110\}_{PA}$ faces. The crystals were cleaved to expose $(111)_{PA}$ and $(10\bar{1})_{PA}$ faces with dimensions of approximately 2×2 mm^2. The diamond-shaped SA crystals were 5−8 mm wide and 1−1.5 mm thick and easily cleaved along $[001]_{SA}$ by applying a razor to the $(100)_{SA}$ face, yielding clean $(010)_{SA}$ surfaces with dimensions of approximately 3×3 mm^2. Crystal face assignments were confirmed by X-ray diffraction.

Methods. Sublimations of **1** were performed under static vacuum (~100 Torr) using an Ace Glass sublimation adapter with a coldfinger (15 °C) and a 100 mL recovery flask. Single crystal substrates were cleaved using a razor blade, mounted with double-sided adhesive tape on a small glass cover slip, and attached to the end of the coldfinger with silicone grease. The substrate crystals were positioned approximately 1 cm from the sublimand, which was heated to 95 °C after the apparatus was evacuated. Deposition times ranged from 15 to 18 h. Their colors, morphologies, micro-Raman spectra, and melting points identified the polymorphs of **1** crystallized on the substrates.[23]

Raman microscopy was performed with a Renishaw System 1000 research model Raman spectrometer utilizing a HeNe laser (632 nm) and a CCD detector, interfaced with an Olympus BH-2 microscope using a 50× objective. Data were collected and processed using GRAMS/32 (Galactic Industries) and Renishaw WIRE software. Spectra were calibrated against the spectrum of cyclohexane. Laser power was attenuated by a series of constant density filters. Spectra were collected as a sum of 5−10 scans, depending on the region of interest.

Optical microscopy was performed using a Zeiss Axioplan polarizing microscope with a Kodak digital camera. Images were collected with a frame grabber and visualized with Adobe Photoshop 5.0. Thermal behavior, including phase transitions and melting, was examined using an Olympus BH-2 microscope equipped with a Linkam TMS93 hotstage. Substrate crystals were indexed by X-ray diffraction with a Siemens Diffractometer D5000 and a Huber four-circle optical goniometer. Crystal habit drawings were generated with SHAPE (Shape Software).

Atomic force microscopy (AFM) was performed with a Digital Instruments Nanoscope III scanning probe microscope, equipped with Nanoscope 4.22 software, a *j*-scanner, and a Si_3N_4 tip with a force constant of 0.12 N/m or a Park Instruments sharpened microlever with a force constant of 0.05 N/m. Images of crystals of **1** were collected directly on the organic acid substrates in air at room temperature using contact force or error modes without filtering and with a look ahead gain of 0.0. Scan rates ranged from 1 to 1.5 Hz with minimal tip forces. AFM goniometry, in which the angles between exposed planes are measured from the line profiles traced by the tip as it is moved across the crystal surface, has been described elsewhere.[25]

Geometric Lattice Modeling

Any substrate/overlayer interface, wherein "overlayer" refers to a crystalline film or a Miller plane of a single crystal contacting the substrate, can be characterized by seven parameters (a_1, a_2, and α_s for the substrate, b_1, b_2, and β_o for the overlayer, and the angle of azimuth θ defining the relative orientation of the two lattices). Both molecular-based potential energy and geometric methods have been used to analyze and explain epitaxial growth of overlayers on crystalline substrates. In both approaches, the interface typically is evaluated by rotating the overlayer lattice relative to the contacting substrate plane over a specified range of θ. Potential energy methods rely on optimal epitaxial configurations from energy minima occurring for a particular substrate/overlayer combination within a specified range of θ, with the interface energy calculated by summation of substrate atom−overlayer atom interaction potentials over a specified interface area. Geometric methods,[26−29] on the other hand, simply rely on analysis of lattice matching, that is, the phase coherence between substrate and overlayer lattices, which makes these computationally more efficient than potential energy calculations. The validity of geometric modeling approaches has been demonstrated by numerous examples of predicted epitaxial configurations (i.e., the azimuthal relationships of overlayer−substrate combinations) that agree with those observed experimentally or deduced by potential energy methods.[30,31]

Examples of geometric models of epitaxy include the reciprocal-space o-lattice formalism of Bollmann[26−28] and a more recent variant referred to as CHASM,[32,33] as well as EpiCalc, a routine previously reported by one of our groups.[29] The Bollman and CHASM models rely on the principle of the "o-lattice", which is constructed from coinciding substrate and overlayer lattice points. The o-lattice of coinciding "o-points" defines the length scale of the phase coherence between the opposing lattices. For cases in which the primitive cell of the overlayer is not commensurate with the substrate, the o-lattice corresponds to a "supercell" comprising an integral number of primitive cells. EpiCalc relies on analysis of lattice coherence, through the superposition of plane waves that reflect the periodicities of the lattices, for a particular substrate/overlayer combination over a specified range of θ. The principal feature of EpiCalc is the calculation of a "dimensionless potential", V/V_o, that achieves discrete values for specific *modes* of epitaxy (i.e., commensurism, $V/V_o = 1.0$; coincidence, $V/V_o = 0.5$; incommensurism, $V/V_o = 0.0$).[34] EpiCalc also allows direct determination of supercell size from the coefficients of a matrix whose elements describe the spatial relationship between the principle substrate and lattice vectors.

The geometric lattice modeling routine described here, which we have dubbed GRACE (global real-space analysis of crystal epitaxy), departs significantly from the previous models. Rather than searching for exact matches between lattices and determining the mode of epitaxy, GRACE takes into account both exact *and* near-coinciding points to produce an "epitaxy score" that reflects the density and precision of lattice coincidence within a predefined search area. That is, GRACE does not require exact registry of overlayer primitive cells or supercells with the underlying substrate, as it will detect slightly incommensurate

(24) Calligaro, D. O.; Fairhurst, J.; Hotten, T. M. *Bioorg. Med. Chem. Lett.* **1997**, *7*, 25−30.
(25) Hillier, A. C.; Ward, M. D. *Science* **1994**, *263*, 1261−1264.
(26) Bollmann, W. *Crystal Defects and Crystalline Interfaces*; Springer-Verlag: Berlin, 1970.
(27) Bollmann, W. *Philos. Mag.* **1967**, *16*, 363.
(28) Bollmann, W. *Philos. Mag.* **1967**, *16*, 383.
(29) Hillier, A. C.; Ward, M. D. *Phys. Rev. B: Condens. Matter* **1996**, *54*, 14037−14051.
(30) Last, J. A.; Hooks, D. E.; Hillier, A. C.; Ward, M. D. *J. Phys. Chem. B* **1999**, *103*, 6723−6733.
(31) Hooks, D. E.; Fritz, T. E.; Ward, M. D. *Adv. Mater*. **2001**, *13*, 227.
(32) Reeves, N. J.; Evans, J. S. *J. Phys. Chem.* **1996**, *100*, 17297.
(33) Reeves, N. J.; Evans, J. S. *J. Phys. Chem. B* **1997**, *101*, 6665.
(34) Rigorous definitions for commensurism, coincidence, and incommensurism recently have been developed and clarified in ref 32. These conditions can be distinguished by the types of numbers (integers, fraction, rational, and irrational) that appear as elements in the 2×2 matrices that describe the relative orientations of overlayer and substrate lattices. Space limitations, however, permit only a qualitative explanation of these conditions. (i) Commensurism exists when all the overlayer lattice points lie simultaneously on *two* primitive substrate lattice lines and coincide with symmetry equivalent substratem, a condition that can also be described as "point-on-point" (POP) coincidence. (ii) The most common form of coincidence, which is prevalent for organic overlayers, is point-on-line coincidence wherein certain [*h, k*] lines of the overlayer coincide with one set of *primitive* substrate lines (i.e., [0, 1]). In this case, a supercell defines the phase-coherent registry with the substrate. (iii) Incommensurism describes a condition wherein no distinctive registry between the substrate lattice and the deposit lattice exists.

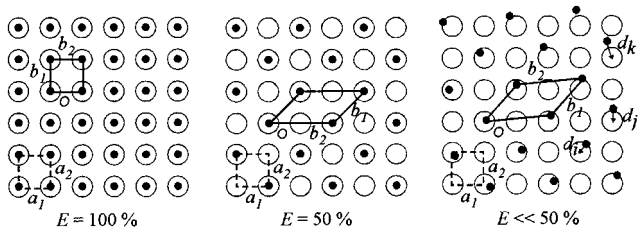

Figure 1. Representative epitaxial configurations for overlayer lattice points (filled circles) on substrate lattice points (open circles). The left and middle panels depict commensurate configurations for which $d_i = 0$ for all overlayer lattice points, but the middle panel has one-half as many substrate lattice points coinciding with overlayer lattice points, affording an E value of 50%. The E score for the version on the right, which is obtained by rotating the overlayer in the middle panel counterclockwise by five degrees, is much less than 50%, owing to the obvious mismatch represented by d_i, d_j, d_k, etc. Such a low E score may be obtained by either rotating an otherwise commensurate lattice to a noncommensurate position or by an overlayer that cannot achieve a high quality of lattice match regardless of azimuthal orientation.

arrangements that are undetected by EpiCalc and o-lattice models. In this respect alone, GRACE resembles the geometric modeling routine used by Hoshino to analyze the organic films on crystalline substrates.[35] Unlike these other routines, GRACE automatically calculates the epitaxy score over a specified range of θ for *all* possible overlayer/substrate combinations for a selected substrate and a user-specified range of *hkl* planes for each polymorph, with these *hkl* planes corresponding to the overlayer in contact with the substrate. The lattice constants of the *hkl* planes for these calculations are automatically generated from the lattice constants of the bulk polymorphs. Thus, GRACE is a convenient approach to assessing the relative effectiveness of different substrates for nucleating desired polymorphs through 2-D epitaxy. The polymorphs typically are selected from known crystallographically characterized forms, but in principle, they can be selected from putative forms generated by empirical crystal modeling methods.

The principal feature of GRACE is the calculation of the epitaxy score E using eq 1, for each substrate/overlayer combination at user-specified increments of θ over a specified range of θ,

$$E = \frac{1}{n}\sum_i \exp(-d_i^2/d_0^2) \times 100 \qquad (1)$$

where i signifies the ith point of the substrate lattice, d_i is the distance between the ith substrate lattice point and a nearby overlayer lattice point, d_0 is an adjustable parameter that governs the sensitivity of E to lattice mismatch (see later), and n is the number of substrate lattice points, which correspond to the cell vertices of the substrate Miller plane, in the predefined search area (Figure 1). After exploring the entire search space (substrates, polymorphs, Miller planes, and azimuthal angles), GRACE produces a final ranking of potential epitaxial matches based on the score E, which can be displayed in tabular or graphical format. The scoring function defined by eq 1 is designed with the following features:

(i) The highest score $E = 100\%$ is achieved if each substrate lattice point coincides with an overlayer lattice point ($d_i = 0$), with the overlayer lattice points corresponding with the vertices of the primitive overlayer unit cell.

(ii) Azimuthal rotation of the overlayer lattice in (i) on the substrate lattice to noncommensurate configurations affords smaller values of E; the sensitivity of E to this rotation is determined by the parameter d_0. This results in a peak in the E versus θ output where $E = 100\%$, with the width of this peak determined by d_0. Though it is possible to use other functions, the Gaussian form of eq 1 was chosen because of its similarity to interatomic potential functions and its sensitivity to lattice mismatch.

(iii) In addition to the misalignment of the substrate and overlayer lattices, the value of E is affected by the inequivalence between overlayer and substrate unit cells, which naturally leads to lower density of coinciding points within a search area. For example, an overlayer cell with the same symmetry and occupancy as the $E = 100\%$ example but with twice the area would lack coincidence with one-half of the substrate lattice points, thereby producing a score of $E = 50\%$. Substantially lower E scores can result if the symmetry of the overlayer, particularly low symmetry overlayers, prevents coincidence of the overlayer lattice points with the lattice points of the substrate.

To improve computational efficiency, GRACE implements a cutoff distance d_c such that any lattice mismatch between a pair of overlayer and substrate lattice points exceeding d_c is ignored. This is equivalent to truncating the Gaussian function in eq 1 at d_c. In this work, we chose $d_c = 0.5$ Å and $d_0 = 0.3$ Å. Under this condition, a slightly missed coincidence with $d_i = 0.5$ Å ($= d_c$) contributes 0.06 to the sum in eq 1, as compared to a contribution of 1.00 from a perfect coincidence ($d_i = 0$). The computational efficiency also depends on the range of θ, the increment of θ, and the search area. The range of θ values depends on the symmetry, but searches are generally performed over the range $-90° \le \theta \le 90°$ to ensure all possible nonredundant configurations have been included. The nonredundant θ range can be reduced to 90° if one of the lattices has square symmetry and to 60° if one of the lattices has hexagonal symmetry. The search area, which must be sufficiently large to eliminate false maxima,[30] can be determined readily by the convergence of the E versus θ profile with increasing area. The optimum values with respect to balancing precision and computational time depend on the particular substrate/overlayer combination, but typically, a θ increment of 0.5° and a search area of 400 Å × 400 Å are sufficient. Computation time is also affected by the user-selected range of overlayer *hkl* planes, though GRACE gains some computational efficiency by excluding from its analysis planes that are redundant by symmetry (e.g., (*hkl*) and ($h\bar{k}l$) of monoclinic crystals need to be analyzed only once). A range of $-3 \le h, k, l \le +3$ is typical and computationally convenient.

Another feature of GRACE is the determination of the metric E/σ for prominent peaks in the E versus θ output plots, where σ corresponds to the standard deviation of the baseline "noise" that is produced by lower-grade lattice matches occurring at nonoptimal orientations. This metric was implemented because reasonable epitaxial conditions may exist, even if the absolute value of E is small. This may occur, for example, when the overlayer unit cells are significantly larger than the substrate unit cells. In such a case, the majority of the substrate lattice points will not coincide with the overlayer lattice points, thereby producing a low E score. Reasonable epitaxy, however, may still be attainable under these conditions. Thus, a low E score with a low σ may correspond to an epitaxial match for one substrate that is as good as one with a high E score and a high σ for another substrate. In this respect, GRACE is most effective and reliable when comparing epitaxy among polymorphs on the same substrate or for a given compound nucleating on different substrates. For a given substrate, it is the *relative* E scores among possible polymorph overlayers that reveal the preferred polymorph and its epitaxial orientation.

Despite their differences, comparisons of results produced by GRACE for configurations with exact registry with those obtained with proven methods such as EpiCalc are useful for establishing the validity of GRACE with respect to predicting and analyzing epitaxial configurations. For example, GRACE predicts the observed epitaxial configuration of the (111) plane of NH_4I on the (001) plane of mica,[36] with $\theta = 0°$ and $E = 46\%$ ($E/\sigma = 154$), which is also identical to the configuration predicted by EpiCalc.[37] Likewise, GRACE finds the observed epitaxial orientation, at $\theta = 20°$ and $E = 1.0\%$ ($E/\sigma = 6.4$), for the low symmetry (001) plane (p1 plane group symmetry) of a β-ET_2I_3 overlayer (ET = ethylenedithiolotetrathiafulvalene) on the basal plane of HOPG (highly oriented pyrolytic graphite).[38,39] This orientation is also predicted by EpiCalc, with the mode of epitaxy identified as coincidence. It is interesting to note that the value of E is quite small for this latter example, even though it forms a coincident lattice with a relatively small 1 × 3 supercell (by EpiCalc), whereas larger values

(35) Hoshino, A.; Isoda, S.; Kurata, H. *J. Appl. Phys.* **1994**, *76*, 4113.

(36) Dunning, J. W. Structure of Surfaces. In *Physics and Chemistry of the Solid State*; Fox, D.; Labes, M. M.; Weissburger, A., Eds.; New York: Interscience, 1965; Vol. I, Chapter 7.

of E can be obtained for incommensurate configurations with other systems (vide infra). This again indicates that GRACE is best used to compare the *relative* quality of epitaxy among polymorphs.

It should be noted that the geometric analysis does not take into account various kinetic factors, such as different inherent nucleation rates of polymorphs, relative growth rates of different crystal planes, Ostwald's rule of stages for polymorph nucleation, and solvent effects. Consequently, a high epitaxy score may not always be a predictor of preferred nucleation. It is more accurate to consider epitaxial matches discovered by GRACE as the *probable* configurations, with the recognition that other factors contribute to the nucleation of the polymorphs.

Results and Discussion

Polymorphs and Substrates. The six polymorphs of **1** can be distinguished by their color and morphology: red prisms (R), orange-red plates (ORP), orange plates (OP), orange needles (ON), yellow needles (YN), and yellow prisms (Y).[23] Control of polymorphism of **1** using conventional crystallization methods is challenging; for example, multiple polymorphs crystallize concomitantly from methanol with selective crystallization achieved only after numerous trials and through careful introduction of seeds of the desired polymorph. Forms YN and ORP are the least stable, transforming to more stable forms in hours to days upon standing at room temperature. Form Y is the most stable form below 70 °C, and ON is the most stable form above 70 °C. The different colors of these polymorphs stem from the different conformations of **1** in the solid state, achieved through torsional rotation about the (phenyl)C−N−C(thiophene)−S segment that produces varying degrees of conjugation between the phenyl and thiophene rings. This conjugation affects the vibrational spectra as well, most notably the ν_{CN} stretching band ($\sim$2220 cm^{-1}) that can be used to identify each polymorph.

Pimelic acid and succinic acid crystals were chosen as substrates in order to compare LDE-driven nucleation to growth governed by 2-D epitaxy. These diacids can be readily grown as large crystals, which can be cleaved to generate well-defined faces decorated with one-dimensional ledges that coincide with one-dimensional chains of hydrogen-bonded HOOC−$(CH_2)_n$−COOH molecules. Each ledge represents the intersection of a well-defined terrace plane and step plane. Because these planes contain the hydrogen-bonded chains, they are characterized by relatively low surface energies and tend to be molecularly smooth over large areas, which can be verified by atomic force microscopy (AFM). Because of their different crystal structures, the ledges on the PA and SA surfaces have different ledge angles, allowing comparisons between the two substrates with respect to ledge geometry and its role in nucleation. Furthermore, the in-plane lattice parameters of the crystal faces of PA and SA differ, permitting examination of the role of two-dimensional epitaxy in nucleation and growth of **1** (Figure 2).

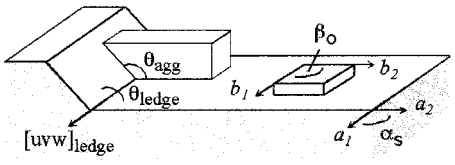

Figure 2. Schematic representation of ledge-directed and two-dimensional epitaxy nucleation on organic crystal substrates. The ledge site of the crystal substrate is denoted according to the direction $[uvw]_{ledge}$, which corresponds to the intersection of a step and terrace plane. The ledge site has a well-defined angle, θ_{ledge}. LDE-driven nucleation is favored if a prenucleation aggregate corresponding to a particular bulk polymorph possesses two low index crystal planes that form a dihedral angle (θ_{agg}) that matches that of the ledge (θ_{ledge}). Two-dimensional epitaxy of a particular polymorph is favored when mismatch between the overlayer and substrate is minimized. The overlayer/substrate interface is described by seven lattice parameters: a_1, a_2, and α_s of the substrate, b_1, b_2, β_o of the nucleant overlayer, and θ, the angle between a_1 and b_1 (not shown). Perfect epitaxy, which would produce an E score of 100% with our geometric lattice modeling routine, would exist when the lattice vectors of the substrate and overlayer coincide exactly and have identical magnitudes such that every overlayer lattice point resides on a substrate lattice point.

Crystallization of 1 on Pimelic Acid. The structure of PA ($HO_2C(CH_2)_5CO_2H$) was reported in 1948[40a] and again later as a different structure. We verified the crystal structure of PA at 100 K and found that it crystallized in the monoclinic space group $C2/c$ with $a = 17.692$ Å, $b = 4.7609$ Å, $c = 9.626$ Å, and $\beta = 106.766°$, in agreement with the more recent report. The structure reveals hydrogen-bonded chains of PA molecules oriented along $[10\bar{1}]_{PA}$, with these chains organized into $(101)_{PA}$ layers through van der Waals contacts (Figure 3).

In our hands, PA crystals grew from aqueous solution as plates with large $\{100\}_{PA}$ faces and smaller $\{101\}_{PA}$, $\{001\}_{PA}$, $\{10\bar{1}\}_{PA}$, and $\{110\}_{PA}$ faces. The crystals are easily cleaved to generate several faces, most prominently $(111)_{PA}$ and $(101)_{PA}$. The latter is the larger face, with dimensions of approximately 2×2 mm^2. The $(101)_{PA}$ surfaces have visible linear features along $[10\bar{1}]_{PA}$, each corresponding to the intersection of a $(101)_{PA}$ terrace and a $(111)_{PA}$ step, generating a $[10\bar{1}]_{PA}$ ledge with $\theta_{ledge} = 123.2°$. Cleavage of the PA crystals along $(111)_{PA}$ is more difficult than along $(101)_{PA}$, and the crystal surface appears rougher by optical microscopy. Nevertheless, the $(11\bar{1})_{PA}$ face also contains visible linear features assignable to $[10\bar{1}]_{PA}$ ledges, with each ledge now consisting of a $(111)_{PA}$ *terrace* and a $(101)_{PA}$ *step*.

To examine nucleation on organic crystal substrates without interference from solvent, the crystal growth experiments described herein were performed by sublimation of **1** onto the substrates. Under these conditions, **1** crystallized on a cleaved $(101)_{PA}$ surface as oriented, yellow, needle-shaped crystals, with >95% of the crystals oriented with their needle axes oriented $90 \pm 0.5°$ with respect to the $[10\bar{1}]_{PA}$ direction (Figure 4). Small ($\sim$2 μm) droplets of supercooled melt (orange color) also formed occasionally on the surface. Under identical conditions, sublima-

(37) The lattice constants for the (111) plane of NH_4I (face-centered sodium chloride structure, space group $Fm3m$, $a = 7.26$ Å) are $b_1 = 10.27$ Å, $b_2 = 10.27$ Å, $\beta_o = 120°$. The specific type of mica used in ref 28 was not given. The epitaxy search described here, however, was performed with paragonite mica [$NaAl_2(AlSi_3O_{10})(OH)_2$], which is monoclinic with $a = 5.13$ Å, $b = 8.89$ Å, $c = 19.32$ Å, and $\beta = 95.17$ (CRC Handbook of Chemistry and Physics). The (001) cleavage plane, which is assumed to be the substrate surface, has lattice constants of $a_1 = 5.13$ Å, $a_2 = 8.89$ Å, and $\alpha_s = 90°$. The epitaxy search yields $E = 50\%$ at $\theta = 0°$ for this mica substrate/NH_4I (111) overlayer combination. Analysis of the same combination with EpiCalc confirms the existence of epitaxy by coincidence, yielding a value of $V/V_o = 0.51$ at $\theta = 0°$. Similar calculations for the (001) cleavage plane of muscovite mica [$KAl_2(AlSi_3O_{10})(OH)_2$], which is monoclinic with $a = 5.18$ Å, $b = 9.02$ Å, $c = 20.04$ Å, and $\beta = 95.5°$, afforded values of $E < 3\%$. Likewise, Epicalc analysis did not produce any rigorously coincident configurations, though a slight expansion of the NH_4I (111) plane ($b_1 = 10.32$ Å, $b_2 = 10.32$ Å, and $\beta_o = 120°$) produced a coincident fit with $V/V_o = 0.51$ at 0.0° and 5.5°.

(38) The lattice constants for the (001) plane of β-ET_2I_3 are $b_1 = 6.61$ Å, $b_2 = 9.10$ Å, and $\beta_o = 109.8°$. The lattice constants for HOPG are $a_1 = a_2 = 2.46$ Å and $\alpha_s = 120°$.

(39) Last, J. A.; Hillier, A. C.; Hooks, D. E.; Maxson, J. B.; Ward, M. D. *Chem. Mater.* **1998**, *10*, 422.

(40) (a) MacGillavry, C. H.; Hoogschagen, G.; Sixma, F. L. J. *Recl. Trav. Chim. Pays-Bas* **1948**, *67*, 869−883. CSD refcode PIMELA01, space group $I2/a$. The other structures reported in the CSD (refcodes PIMELA, PIMELA02) correspond to the high-temperature form of pimelic acid. (b) Thalladi, V. R.; Nüsse, M.; Boese, R. *J. Am. Chem. Soc.* **2000**, *122*, 9227.

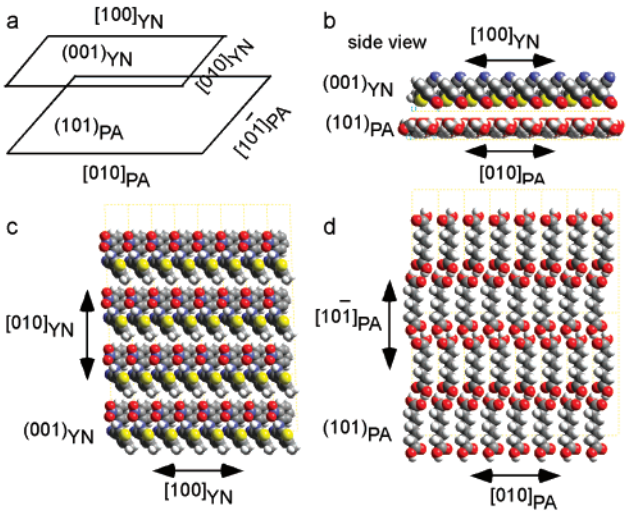

Figure 3. (a) Schematic representation of the $(001)_{YN}/(101)_{PA}$ interface, denoting the planes and directions in the observed alignment. (b) Molecular model of the $(001)_{YN}/(101)_{PA}$ interface as viewed from its side, parallel to the interface. (c) View of the $(001)_{YN}$ that contacts the $(101)_{PA}$ plane, which is illustrated in (d).

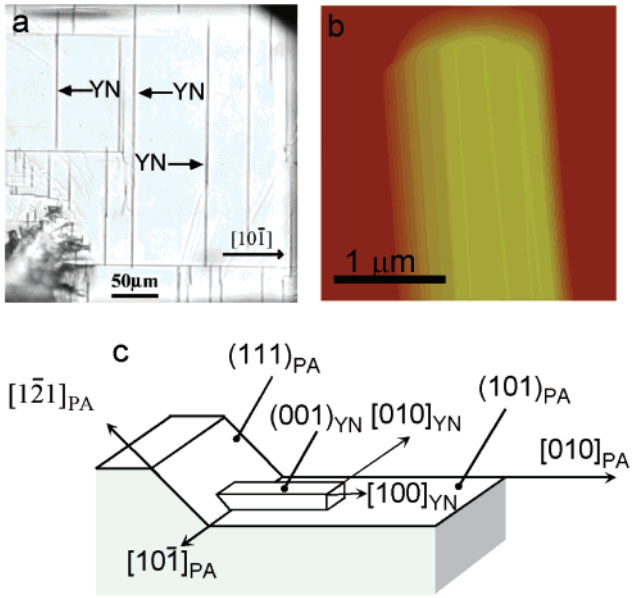

Figure 4. (a) Photomicrograph of highly oriented YN crystals grown by sublimation on a cleaved $(101)_{PA}$ surface of a single crystal of pimelic acid. Some of the YN crystals, all of which are oriented vertically perpendicular to $[10\bar{1}]_{PA}$, are indicated by the arrows. (b) AFM image of a YN crystal on the $(101)_{PA}$ surface. (c) Schematic representation of the YN crystal orientation on the $(101)_{PA}$ face as determined by AFM goniometry (also see Figure 9). The YN crystals grow with the $[100]_{YN}$ needle direction perpendicular to the $[10\bar{1}]_{PA}$ ledge with the $(001)_{YN}$ face contacting $(101)_{PA}$. Though the YN crystals appear to contact the $[10\bar{1}]_{PA}$ ledge, there is no reasonable LDE match for the YN crystals with this ledge (see text).

tion of **1** on a glass slide afforded droplets of the orange supercooled melt and, occasionally, small unoriented curved crystals of form ON. Raman microscopy of yellow crystals grown on the $(101)_{PA}$ faces revealed a ν_{CN} stretch at 2221 cm^{-1}, confirming the identity of the crystals as form YN.[23] Because the YN crystals were mechanically fragile, the Raman spectra were acquired with the YN crystals still adhered to the $(101)_{PA}$ faces. The crystals and the melt droplets completely sublime from the $(101)_{PA}$ surface within one week of storage at ambient temperatures, requiring all measurements of crystal properties to be performed immediately after growth. Under identical conditions, the growth of YN crystals on $(111)_{PA}$ faces was negligible. The relatively few crystals that did form on the $(111)_{PA}$ faces did not exhibit preferred orientations, and optical microscopy revealed that these crystals were orange needles that grew from macroscopic defects on the substrate surface.

Upon gradual heating (5 °C/min), the YN crystals on the $(101)_{PA}$ surface exhibit a phase transition between 70 and 80 °C, followed by rapid sublimation near 90 °C. A few YN crystals remain unsublimed upon rapid heating (20 °C/min); these melt at 99 °C, the same melting point surmised previously by extrapolation of eutectic melting data.[23] Though pimelic acid undergoes a phase transition at 75 °C at which the crystals become opaque,[41] the remaining crystals of YN on the PA surface remain adhered and unchanged during this transition. Notably, bulk YN crystals convert to forms Y and R at room temperature within days and sometimes hours. The YN crystals on the pimelic acid surface, however, slowly sublime from the PA surface over a period of days at room temperature *without* a phase transition. This suggests that the small YN crystals immobilized on the $(101)_{PA}$ substrate have fewer defects (which can initiate phase transitions) than crystals grown directly from solution. Alternatively, the YN form may be stabilized by adhesion to the $(101)_{PA}$ surface.

The epitaxial orientation of the YN crystals on the $(101)_{PA}$ surfaces could not be determined by conventional optical goniometry or X-ray diffraction owing to their small size (ranging from 0.6 to 1.2 μm wide and 400−800 nm high). Therefore, the YN crystals were indexed by AFM goniometry (see Experimental Section), in which the angles between crystal faces are measured with a scanning atomic force microscope tip. This procedure enables assignment of the faces of very small crystals and determination of crystal orientation with respect to the substrate (Figure 4b). Analysis of the adhered YN crystals, based on the known crystal structure of YN,[42] with this method revealed that the $(001)_{YN}$ plane contacts the $(101)_{PA}$ surface (Table S1, Supporting Information; also see Figure 9). The $(001)_{YN}$ plane contains two principal lattice vectors, $[100]_{YN}$ and $[010]_{YN}$, the former coinciding with the needle axes of the YN crystals. The AFM goniometry revealed that the $[100]_{YN}$ and $[010]_{YN}$ directions were parallel to $[010]_{PA}$ and $[10\bar{1}]_{PA}$, respectively (expressed by the formalism $[100]_{YN}||[010]_{PA}$ and $[010]_{YN}||[10\bar{1}]_{PA}$).

The determination of the crystal orientation allows elucidation of the epitaxial mechanism responsible for the observed orientation and polymorph selectivity. Because the YN crystals are oriented with $[010]_{YN}||[10\bar{1}]_{PA}$ and the $(001)_{YN}$ plane in contact with $(101)_{PA}$, any plane contacting the $(111)_{PA}$ step face of the $[10\bar{1}]_{PA}$ ledge must belong to $(h0l)$. Previous work from one of our laboratories revealed that a difference between θ_{agg} and θ_{ledge} of as little as 1° was sufficient to make LDE inactive for a particular combination of planes. An analysis of $(h0l)_{YN} \cap (001)_{YN}$ combinations ($\cap$ here denotes the intersection of the two planes) for h, $l < 5$ produces only one θ_{agg}, $(305)_{YN} \cap (001)_{YN}$, near that of $\theta_{ledge} = 123.2°$ for $[10\bar{1}]_{PA}$ (Table S2). Inspection of the YN crystal structure, however, reveals that$(305)_{YN}$ plane is not densely packed, a characteristic that is important for optimum dispersive interactions with the substrate

(41) Kay, M. I.; Katz, L. *Acta Crystallogr.* **1958**, *11*, 289−294.
(42) YN crystallizes in the triclinic space group P$\bar{1}$ with $a = 4.5918$ Å, $b = 11.249$ Å, $c = 12.315$ Å, $\alpha = 71.194°$, $\beta = 89.852°$, and $\gamma = 88.174°$ (see ref 23).

ledge in the LDE mechanism. Likewise, inspection of the other combinations does not suggest any other higher index $(h0l)_{YN} \cap (001)_{YN}$ combinations with this character. This argues that the LDE is not responsible for the selective nucleation and crystal orientation of the YN form on the $(101)_{PA}$ surface. The absence of growth on the cleaved $(111)_{PA}$ face, *which is also decorated with* $[10\bar{1}]_{PA}$ *ledges* (vide supra), is further evidence that LDE is not responsible for nucleation on the $(101)_{PA}$ face. These observations instead suggest that nucleation is driven by 2-D epitaxy, wherein lattice mismatch in the substrate−nucleant interface is minimized, thereby reducing the activation energy for nucleation of the observed polymorph in the preferred orientation to a greater extent than other polymorphs or nonepitaxial orientations.

Though no reasonable LDE match exists, a substantial number of the oriented YN crystals in Figure 4a appear to emanate from macroscopic $[10\bar{1}]_{PA}$ ledges. This suggests that nucleation of YN driven by 2-D epitaxy may be assisted by nonspecific "wetting" of both planes of the ledge. Optical microscopy cannot discern whether the YN crystals actually contact the ledge or actually begin growing at the ledge. The absence of a reasonable LDE condition, however, suggests that crystallization of YN on $(101)_{PA}$ may be governed solely by 2-D epitaxy, with the ledges simply serving as a physical barrier to further growth along the needle axis.

The role of 2-D epitaxy on polymorphic and surface selectivity was confirmed through a systematic search using GRACE, the geometric lattice modeling routine described above. This search was performed for combinations of the selected substrate planes and lattice planes of the six polymorphs of **1**. The range of polymorph overlayer planes examined was $-3 \le h, k, l \le +3$, and the interface area for the search was 400 Å × 400 Å. As described above, GRACE produces an epitaxy score, *E*, that reflects the degree of lattice match between two contacting substrate and overlayer lattice planes. The search (Figure 5) reveals a prominent peak $\theta = 0°$ with $E = 7.6\%$, where θ is the angle between $[010]_{PA}$ and $[100]_{YN}$. This corresponds to a $(001)_{YN}/(101)_{PA}$ interface with $[100]_{YN}$ parallel to $[010]_{PA}$ and perpendicular to $[10\bar{1}]_{PA}$ and with $[010]_{YN}$ nearly parallel to $[10\bar{1}]_{PA}$, *the experimentally observed orientation*. In more conventional terms, this orientation corresponds to lattice mismatches between nearly coinciding substrate and overlayer lattice vectors of 2.45% for $[100]_{YN}||[010]_{PA}$ and 0.22% for $[020]_{YN}||[10\bar{1}]_{PA}$.[43] The locations of the nearly coinciding lattice points ($d < 0.5$ Å) of the $(001)_{YN}/(101)_{PA}$ interface at $\theta = 0°$ are depicted in Figure 5b. An illustration of these points over the entire 400 Å × 400 Å search area generates a one-dimensional Moiré pattern that is a signature of registry between the two lattice planes along one dimension of reciprocal space (Figure 5c). It should be noted that the $(001)_{YN}/(101)_{PA}$ interface cannot be described as strictly coincident, as the observed and calculated configuration does not produce a finite supercell with vertices that coincide precisely with the substrate. Such a configuration would require some reorganization of the $(001)_{YN}$ plane.

As explained in the modeling section above, the search area used in the GRACE routine represents a compromise between computational time and the avoidance of false maxima. The optimum choice of search area depends somewhat on the particular system under examination, but it can be deduced by examining the convergence of the *E* versus θ output for increasingly larger search areas. This is illustrated in Figure 6 for the $(001)_{YN}/(101)_{PA}$ interface, where two prominent peaks are observed in the vicinity of $\theta = 0°$ for small search areas, but only one dominant peak at $\theta = 0°$, corresponding to the experimentally observed orientation, is observed for large search areas. Notably, the *E* scores decline somewhat with increasing search area, but the E/σ values (see modeling section, above) for the $\theta = 0°$ peak, where σ is the standard deviation of the *E* values at other values of θ in the "baseline", *increase* substantially with increasing search area because of a reduction of σ. This supports the assignment of the $\theta = 0°$ peak to the optimum epitaxial configuration.

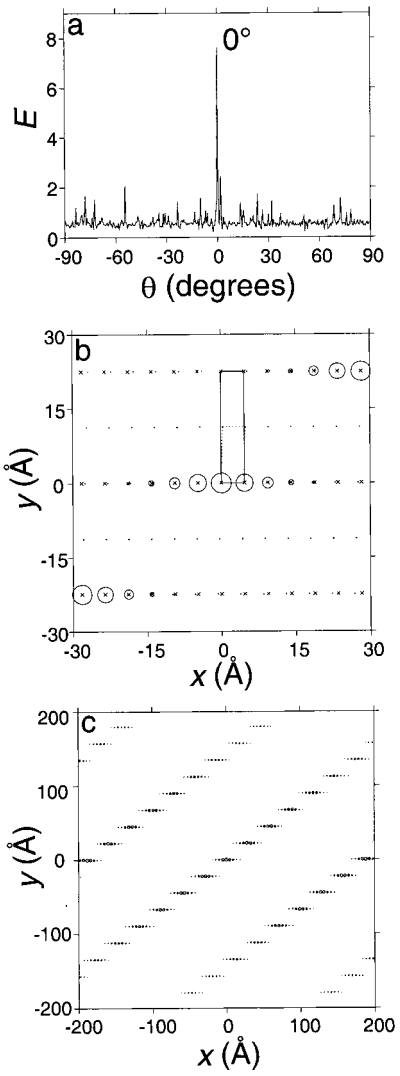

Figure 5. (a) *E* vs θ plot for the $(101)_{PA}/(001)_{YN}$ interface revealing an epitaxial match at $\theta = 0°$, where θ is the angle between $[010]_{PA}$ and $[100]_{YN}$. (b) 60 Å × 60 Å region of the $(001)_{YN}/(101)_{PA}$ interface at $\theta = 0°$. The dots indicate the $(101)_{PA}$ lattice points, and the crosses the $(001)_{YN}$ lattice points. The solid line traces the $(101)_{PA}$ unit cell, and the dotted line the $(001)_{YN}$ unit cell. The *x*- and *y*-directions are parallel to $[010]_{PA}$ and $[10\bar{1}]_{PA}$ vectors, respectively. Nearly coinciding points satisfying the condition $d < d_c = 0.5$ Å are marked with circles whose diameters are proportional to their contributions to the epitaxy score *E*. (c) Schematic representation of a 400 Å × 400 Å region (the actual size of the interface area used in the epitaxial search) of the nearly coinciding lattice points of the $(001)_{YN}/(101)_{PA}$ interface at $\theta = 0°$. This reveals a one-dimensional Moiré pattern that is a signature of the registry between the two lattice planes. The lattice parameters for $(001)_{YN}$ are $b_1 = 4.5918$ Å, $b_2 = 11.249$ Å, $\beta_o = 88.174°$; lattice parameters for $(101)_{PA}$ are $a_1 = 4.7069$, $a_2 = 22.449$, $\alpha_s = 90°$.

(43) For crystals of X and substrate Y, % mismatch = (|(lattice constant)$_X$−(lattice constant)$_Y$|/(lattice constant)$_Y$) × 100. From Pashley, D. W. *Adv. Phys.* **1956**, *5*, 173−240.

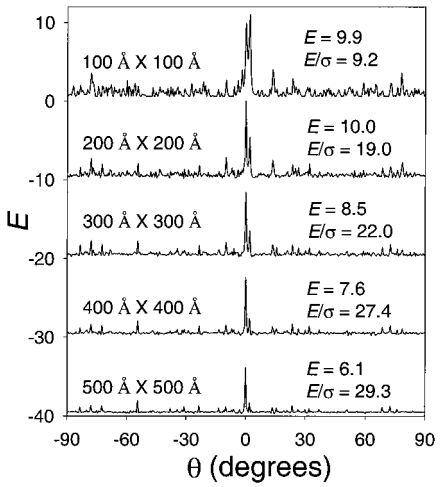

Figure 6. E vs θ output for the $(001)_{YN}/(101)_{PA}$ interface calculated with GRACE for different search areas. E and E/σ values are denoted on each plot.

The values of E and E/σ at $\theta = 0°$ for the $(001)_{YN}/(101)_{PA}$ reflect a reasonably high degree of epitaxy (see above). These values are significantly higher than any observed for the other five polymorphs on $(101)_{PA}$, using the previously reported lattice parameters for each polymorph.[44] That is, among all the crystal planes in the range $-3 \leq h, k, l \leq +3$ for all polymorphs of **1**, the best match to $(101)_{PA}$ is clearly achieved by $(001)_{YN}$. Furthermore, the calculated match for the $(001)_{YN}/(101)_{PA}$ interface exceeds that achieved by any of the *six* polymorphs on the $(111)_{PA}$ surface (Figure 7). Therefore, the experimental observations can be reasonably explained by the geometric modeling with GRACE, demonstrating that 2-D epitaxy governs the observed polymorph *and* substrate surface selectivity.

Crystallization of 1 on Succinic Acid. Succinic acid crystallizes from aqueous solution in the monoclinic space group $P2_1/c$ ($a = 5.519$ Å, $b = 8.862$ Å, $c = 5.101$ Å, $\beta = 91.6°$)[45] as diamond shaped plates with large $\{100\}_{SA}$ faces and smaller $\{010\}_{SA}$, $\{111\}_{SA}$, and $\{001\}_{SA}$ faces. The SA molecules form hydrogen-bonded chains along $[10\bar{1}]_{SA}$, the chains organized in $(010)_{SA}$ layers through van der Waals contacts. The crystals are easily cleaved along $[001]_{SA}$ by applying a razor to the $(100)_{SA}$ face, yielding clean $(010)_{SA}$ surfaces of approximately 3×3 mm^2. These faces contain features along $[10\bar{1}]_{SA}$ that correspond to macroscopic ledges, comprising $(010)_{SA}$ terraces and $(111)_{SA}$ steps, and having a ledge angle of $\theta_{ledge} = 112.6°$. This value is very near that of $(10l)_{YN} \cap (001)_{YN}$ ledge angle ($\theta_{agg} = 111.8°$), suggesting a possible role for LDE-driven nucleation.

Periodic observation of a freshly cleaved $(010)_{SA}$ surface during sublimation of **1** revealed fine yellow needles and red plates on the substrate surface (Figure 8). These forms were accompanied by large droplets of orange supercooled melt, particularly under conditions of fast sublimation. Prolonged sublimation afforded only marginal growth of the red plates (herein referred to as the RPL crystals) but significant growth of the yellow needles. The melt droplets and the RPL crystals gradually sublimed off the $(010)_{SA}$ surface at room temperature at rates exceeding the sublimation of the YN needles from this surface. The RPL crystals melted at 62−63° with slow heating (1 °C/min), but with fast heating, some of the RPL crystals transformed into form YN, as verified by optical microscopy, Raman spectroscopy, and melting point determination. The direct observation of this phase transition suggests that the YN needles observed after prolonged sublimations may result from transformation of RPL crystals formed initially on the substrate surface. Oriented orange needles also appeared on the $(010)_{SA}$ surface after prolonged sublimation, some of which appeared to grow from the melt droplets. Storage at $T < 10$ °C resulted in the growth of unoriented crystals of form R from the melt droplets.

In contrast to the YN needles on the $(101)_{PA}$ surface, the YN needles generated from the RPL phase on $(010)_{SA}$ exhibited *three* different orientations as determined by AFM goniometry: (i) $[100]_{YN}$ parallel to $[100]_{SA}$ and 46 ± 1.5° from the $[10\bar{1}]_{SA}$ ledge direction, (ii) $[100]_{YN}$ parallel to $[001]_{SA}$ and 42 ± 1.2° from the $[10\bar{1}]_{SA}$ ledge, and (iii) $[100]_{YN}$ parallel to the $[10\bar{1}]_{SA}$ ledge. The majority of the crystals exhibited orientation (i). The YN crystals on the $(010)_{SA}$ surface began to sublime at approximately 90° with rapid heating, did not change form when adhered to the substrate surface, and melted at about 99 °C, identical to the behavior observed for this phase on the $(010)_{PA}$ surface. Measurement of the interplanar angles by AFM goniometry revealed that the $(001)_{YN}$ face was in contact with $(010)_{SA}$ regardless of its azimuthal orientation (Figure 9). Unlike $(001)_{YN}$ on $(101)_{PA}$, GRACE did not detect any prominent epitaxial orientations with a high E score, nor any orientations with modest E scores that agreed with the observed orientations. That is, GRACE revealed multiple possible matches of the polymorphs to the $(010)_{SA}$ substrate, but none of these is significantly better than the others, and all of these are significantly worse than the $(001)_{YN}/(101)_{PA}$ match at $\theta = 0°$ (Figure 5c). The larger number of calculated matches (albeit poorer ones) for $(010)_{SA}$ compared to $(101)_{PA}$ most likely reflects the smaller lattice parameters for $(010)_{SA}$, which would tend to increase the chances of an epitaxial match with any organic nucleant. These calculations are consistent with the observation of multiple polymorphs of **1**, including YN, ON, R, and the previously unknown RPL form, on $(010)_{SA}$. The observation of these polymorphs and their multiple orientations on $(010)_{SA}$ suggests that 2-D epitaxy does not govern nucleation. Instead, kinetic effects (e.g., LDE, simple wetting, and the Ostwald's rule of stages) may influence the nucleation of polymorphs.

The observation of multiple orientations of the YN crystals on $(010)_{SA}$ also suggests that a *selective* LDE mechanism was not operative. Indeed, a search for possible LDE matches that included $\{hkl\}_{YN}$ for orientations (i) and (ii), and $\{0kl\}$ for orientation (iii), produced only one combination, $(001)_{YN} \cap (122)_{YN}$, that closely matched the SA ledge ($\theta_{agg} = 112.2°$, $\theta_{ledge} = 112.6°$). Interestingly, the angle formed by $(100)_{YN} \cap (122)_{YN}$ is 45°(or its complement 135°), which is equivalent, within measurement error, to the angles between the $(100)_{YN}$ and the $[10\bar{1}]_{SA}$ for orientations (i) and (ii). This suggests that LDE may play a role in oriented nucleation of some YN crystals as they evolve from the RPL phase. No LDE match exists for orientation (iii). The growth of these YN crystals along the ledge, however, may simply reflect nonspecific wetting of the ledge site at some

(44) Y: $P2_1/n$, $a = 8.5001$ Å, $b = 16.413$ Å, $c = 8.5371$ Å, $\alpha = 90°$, $\beta = 91.767°$, $\gamma = 90°$. ON: $P2_1/c$, $a = 3.9453$ Å, $b = 18.685$ Å, $c = 16.3948$ Å, $\alpha = 90°$, $\beta = 93.830°$, $\gamma = 90°$. OP: $P2_1/n$, $a = 7.9760$ Å, $b = 13.319$ Å, $c = 11.676$ Å, $\alpha = 90°$, $\beta = 104.683°$, $\gamma = 90°$. R: $P\bar{1}$, $a = 7.4918$ Å, $b = 7.7902$ Å, $c = 11.9110$ Å, $\alpha = 75.494°$, $\beta = 77.806°$, $\gamma = 63.617°$. YN: $P\bar{1}$, $a = 4.5918$ Å, $b = 11.249$ Å, $c = 12.315$ Å, $\alpha = 71.194°$, $\beta = 89.852°$, $\gamma = 88.174°$. ORP: $Pbca$, $a = 13.177$ Å, $b = 8.0209$ Å, $c = 22.801$ Å, $\alpha = 90°$, $\beta = 90°$, $\gamma = 90°$ (see ref 23).

(45) Leviel, J.-L.; Auvert, G.; Savariault, J.-M. *Acta Crystallogr.* **1981**, *B37*, 2185−2189.

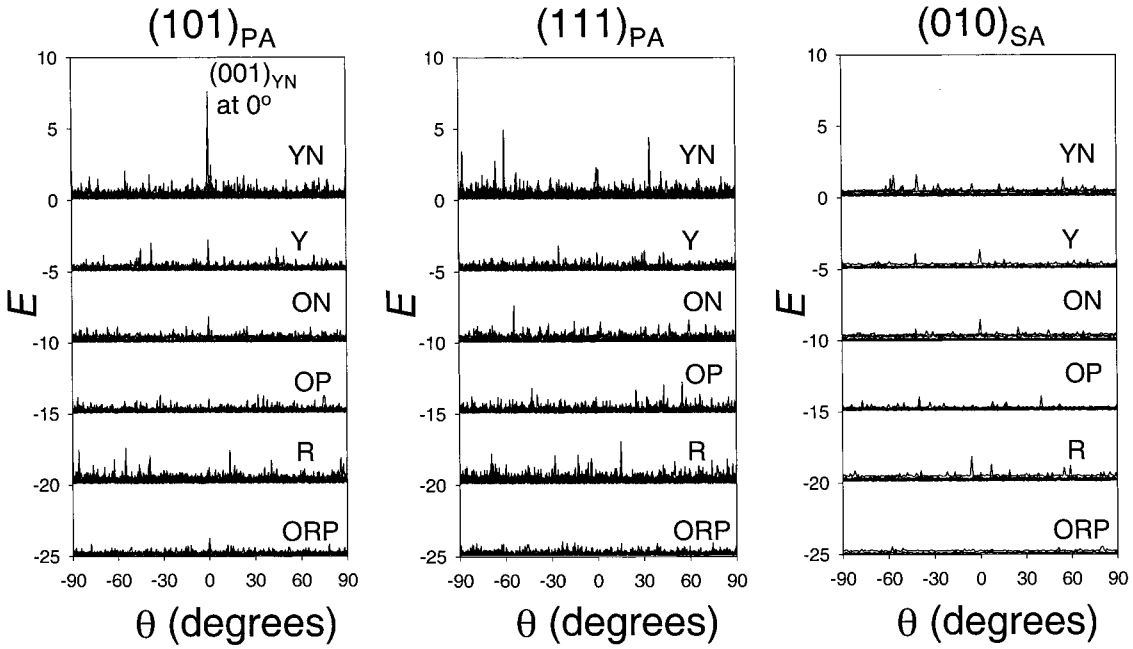

Figure 7. Representative comparisons of lattice matching between the prominent PA and SA substrate surfaces and the polymorphs of **1** as determined with the geometric lattice modeling routine GRACE. Each panel depicts the E vs θ plots for one substrate (identified at the top). Within each panel, the results for the different polymorphs are displaced so that each can be observed independently. The outputs for all the substrate/overlayer hkl combinations are overlaid for each polymorph. Though for each polymorph the search was performed in the range $-3 \leq h, k, l \leq +3$, the output illustrated here is limited to the range $-1 \leq h, k, l \leq +1$ for clarity. Searches outside this range did not produce any appreciable E scores. The $(001)_{YN}/(101)_{PA}$ combination at $\theta = 0°$ represents the best epitaxial match ($E = 7.6\%$ and $E/\sigma = 27.4$) among all the possibilities, in agreement with the experimental results. The calculations were performed with a search area of 400 Å × 400 Å and θ increment of 0.5°, using the previously reported lattice parameters for each polymorph.

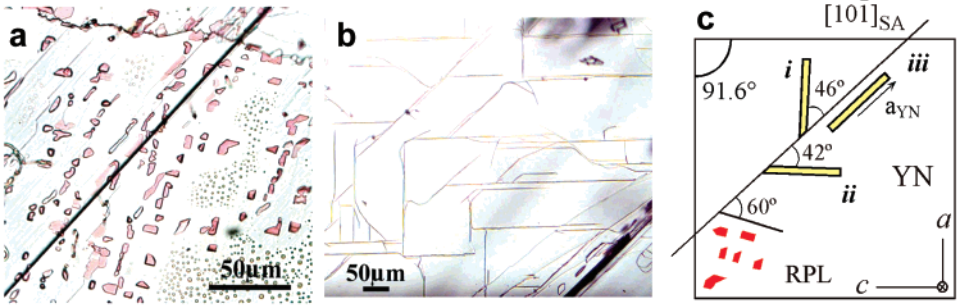

Figure 8. (a) Photomicrograph of form RPL on a cleaved $(010)_{SA}$ surface. The dark line highlights a $[10\bar{1}]_{SA}$ ledge. (b) Photomicrograph of YN crystals on the cleaved $(010)_{SA}$ surface, formed after prolonged sublimations. (c) Schematic representation of the YN crystal orientations (i), (ii), and (iii) on the $(010)_{SA}$ surface.

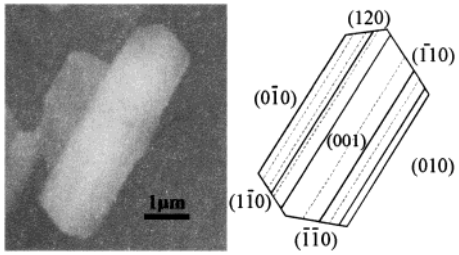

Figure 9. AFM image and cross-section of a YN crystal adhered to the $(010)_{SA}$ surface. The surface profile and perimeter angles were used to assign the crystal facets and the orientation of the YN crystals on the SA substrate. An identical procedure was used for the YN assignment in Figure 4.

stage in crystal growth (in contrast to LDE, which is based on intimate contact of two crystal planes of the nucleus with the ledge site during nucleation). Like LDE the nonspecific wetting at a ledge can be driven by a greater reduction in surface energy, compared with growth limited to only the terrace.

The RPL phase adhered to the SA surface appeared crystalline, with 90° angles between at least two sides and many exhibiting a rectangular habit. Over 95% of the crystals had one of the crystal edges oriented 60 ± 1° with respect to the $[10\bar{1}]_{SA}$ ledge. Though this would appear to suggest a single orientation, polarized light microscopy of the RPL crystals adhered to the SA surface revealed dichroic behavior associated with two mutually perpendicular orientations of the RPL crystals. The observation of this dichroism also confirms that the red plates are indeed crystalline. The Raman spectrum of the RPL crystals is similar overall to that of form R but differs with respect to two ν_{CN} stretches observed at 2210 and 2215 cm^{-1} as compared to the single peak observed at 2212 cm^{-1} for form R. All the other polymorphs exhibit single ν_{CN} absorption peaks, suggesting the existence of multiple conformers in the RPL phase. The RPL crystals also differ from form R with respect to melting point, the R phase melting at 106.2° rather than 63° for the RPL crystals. Furthermore, form R is triclinic, and consequently, its crystals would not likely exhibit the 90°

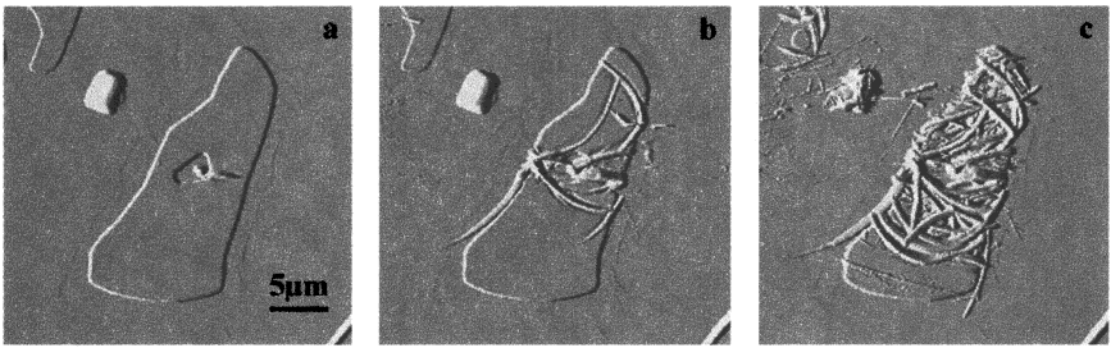

Figure 10. AFM image of single crystals of RPL on the $(010)_{SA}$ face, taken at 8-minute intervals. Raster scanning of the tip across the crystal causes a polymorphic transformation to form YN.

profile angles observed for the red plates. In addition, the RPL crystals are less stable than YN crystals, whereas R has been shown to be more stable than YN.[23] These observations establish that RPL is a new polymorph of **1**, though this form is unstable and observed only when adhered to the $(010)_{SA}$ surface.

Contact mode AFM imaging of the RPL crystals revealed crystal dimensions of approximately 1−20 μm wide and 200 nm−1 μm tall. The interfacial angles between the large upper face of an RPL crystal and its adjoining side faces were steeper than 129°, the lower limit for measurement with the AFM tips used in this investigation. Surprisingly, contact mode imaging caused a phase transition from form RPL to YN (Figure 10). This transformation, which was verified by Raman spectroscopy, was apparently induced by the mechanical pressure exerted by the AFM tip in contact mode. This prevented acquisition of lattice images that would have enabled more detailed structural characterization of the RPL crystals and determination of their orientation on the substrate. Acquisition of lattice images of the RPL surface was attempted in polar liquids, wherein a reduced Hamaker constant generally reduces capillary and tip−sample forces.[46] These attempts were not successful, owing to dissolution of the RPL crystals, even in very concentrated solutions of **1**. Consequently, the lattice orientation of the RPL crystals and the mode of epitaxy responsible for their selective nucleation remains unknown. Attempts to grow macroscopic RPL crystals for X-ray diffraction, using the crystals adhered to the $(010)_{SA}$ surface as seeds, were unsuccessful because of the small number of RPL crystals present and its high solubility in both polar and nonpolar solvents.

Conclusion

This investigation has revealed two interesting features: (i) only polymorph YN, a metastable member of the now heptamorphic crystal system of **1**, nucleates on the PA substrate, and (ii) YN crystal growth occurs selectively on the $(101)_{PA}$ plane because of 2-D epitaxy. A comprehensive search for 2-D epitaxy using a geometric lattice modeling routine indicates that the $(001)_{YN}$ plane has, by far, the best reasonable match to the $(101)_{PA}$ surface among the six structurally characterized polymorphs of **1**, but none of the polymorphs have an epitaxial match with the $(111)_{PA}$ surface. This explains the selectivity for the YN form by the PA substrate as well as the selectivity for growth on the $(101)_{PA}$ surface.

In comparison, the $(010)_{SA}$ substrate is less selective, promoting the nucleation of several polymorphs, including a new metastable RPL form. Multiple orientations of the RPL and YN forms are also observed on this surface. The lack of polymorphic and orientational selectivity on $(010)_{SA}$ is explained by the geometric lattice analysis, which reveals poor epitaxial matches between $(010)_{SA}$ and several polymorphs of **1** but no inherent selectivity toward a single polymorph. Unfortunately, the instability of the RPL polymorph prevented the detailed characterization necessary for establishing its orientation with respect to the substrate and the mode of epitaxy responsible for its formation.

This investigation demonstrates that crystal nucleation and polymorph selectivity are highly sensitive to the substrate surface. Polymorph selectivity can be achieved through two-dimensional epitaxy, which allows efficient screening of substrates for polymorph control through geometric lattice modeling prior to performing experiments with actual libraries. Though the experiments here were performed using sublimation, the use of organic crystal substrates for polymorph control can be extended more generally to liquid phase crystallizations, as demonstrated previously by one of our groups.[20] Furthermore, it is likely that these concepts can be extended readily to inorganic materials with a natural layered character; such substrates may be advantageous with respect to their reduced general solubility relative to their organic counterparts. The unanticipated discovery here of a new polymorph also demonstrates that searches for unknown polymorphs can be assisted by the use of substrate libraries.

Acknowledgment. We would like to thank Julie Last and Dan Hooks for assistance with the AFM studies, Susan Reutzel-Edens for valuable discussions, Greg Stephenson, Ray Childers, and Jim Osborne for analytical assistance, and Mr. Jiaoming Qiu for helpful comments. The authors also acknowledge the financial support of Eli Lilly, the University of Minnesota Industrial Partnership for Interfacial and Materials Engineering (IPRIME), and the University of Minnesota NSF Materials Research Science and Engineering Center (under Grant DMR-9809364).

Supporting Information Available: Tables of crystal plane dihedral angles and crystal data, structure solution and refinement, positional parameters, and anisotropic thermal parameters for pimelic acid (5 pages, PDF). This material is available free of charge via the Internet at http://pubs.acs.org. GRACE is available, in an executable file format, from the authors upon request.

JA004085F

(46) Israelachvilli, J. *Intermolecular and Surface Forces*; Academic Press: New York, 1992.